JOURNAL OF AIRCRAFT
Vol. 40, No. 1, January–February 2003

Oscillating Turntable for the Measurement of Unsteady Aerodynamic Phenomena

David J. Piatak* and Craig S. Cleckner†
NASA Langley Research Center, Hampton, Virginia 23681

A new forced oscillation system has been installed and tested at NASA Langley Research Center's Transonic Dynamics Tunnel. The system is known as the Oscillating Turntable (OTT) and has been designed for the purpose of oscillating, large semispan models in pitch at frequencies up to 40 Hz to acquire high-quality unsteady pressure and loads data. Precisely controlled motions of a wind-tunnel model on the OTT can yield unsteady aerodynamic phenomena associated with flutter, limit-cycle oscillations, shock dynamics, and nonlinear aerodynamic effects on many vehicle configurations. This paper will discuss the general design and components of the OTT and will present data from performance testing and from research tests on two rigid semispan wind-tunnel models. The research tests were designed to challenge the OTT over a wide range of operating conditions while acquiring unsteady pressure data on a small rectangular supercritical wing and a large supersonic transport wing. These results will be presented to illustrate the performance capabilities, consistency of oscillations, and usefulness of the OTT as a research tool.

Nomenclature

C_p/deg	=	pressure coefficient normalized by oscillation amplitude
$(C_p)_{\mathrm{Im}}$/deg	=	imaginary component of pressure coefficient normalized by oscillation amplitude
$(C_p)_{\mathrm{mean}}$	=	mean pressure coefficient
$(C_p)_{\mathrm{Re}}$/deg	=	real component of pressure coefficient normalized by oscillation amplitude
f	=	frequency, Hz
k	=	reduced frequency
M	=	Mach number
Q	=	dynamic pressure, psf
Re	=	Reynolds number
x/c	=	nondimensional chordwise location
$\bar{\alpha}$	=	mean angle of attack, deg
$\lvert\alpha\rvert$	=	angular amplitude, deg
ΔP	=	hydraulic pressure amplitude, psi

Introduction

TODAY, an aircraft's structure tends to be conservative in strength for many reasons, including the lack of accurate flutter prediction codes. If one can accurately predict the flutter and other aeroelastic characteristics of an aircraft before it is constructed, the aircraft wing structure could be optimized from the perspectives of flutter, strength, and weight. However, many incidences of aeroelastic shortcomings are identified and addressed after an aircraft's first flight because of the challenges, especially in the transonic regime, of predicting the complex interaction of aerodynamic forces, elastic forces, and inertial forces. Accurate aeroelastic analyses require rigorous modeling of the unsteady aerodynamic environment at transonic speeds and high reduced frequencies.

There are many phenomena associated with aeroelasticity that challenge today's aeroelastic analysis methods, particularly the components of these analyses simulating vehicle aerodynamics. At transonic speeds steady and unsteady aerodynamic effects tend to reduce the flutter dynamic pressure of a vehicle and are difficult to predict accurately. Other challenging unsteady flow phenomena include shock dynamics, shock-induced flow separation, flow associated with limit-cycle oscillations (LCO), vortical flow caused by high incidence angle and configuration, and various other nonlinear unsteady aerodynamic effects. To achieve the goal of improving the prediction of flutter and other aeroelastic phenomena for future aircraft designs, advancements must be made in the prediction of unsteady pressures and the resulting loads on configurations oscillating at high reduced frequencies and at transonic speeds.[1–3]

Validation of and improvements to unsteady aerodynamic analysis methods require experimental benchmark data for correlation. To acquire such data, unsteady pressure measurements are typically made on subscale wind-tunnel models while undergoing flutter or during forced oscillations. There have been several studies that have measured unsteady pressures and loads on wind-tunnel models undergoing forced oscillations. References 4–7 present such results from semispan rectangular planform wind-tunnel models at frequencies up to 60 Hz, but these experiments were limited to small, rectangular wings with low pitch inertias. Reference 8 presents unsteady pressure and loads data from a relatively small, straked delta-wing model oscillated in pitch at frequencies up to 16 Hz. The majority, however, of available unsteady pressure data have been acquired during flutter at frequencies on the order of 10 Hz or less.[9–11] Under these conditions the out-of-phase component of pressure is typically small and difficult to measure accurately. Many unsteady computations do not compare well with measured data for the out-of-phase component of pressure. With the given data it is difficult to determine if this is a shortcoming of the theoretical methods employed or errors in the measurements caused by small-amplitude pressure fluctuations. Tests at higher frequencies and oscillation amplitudes should result in larger, more accurately measured, out-of-phase pressure amplitudes that will help answer these questions. Therefore, the ability to oscillate large wind-tunnel models in pitch at a wide range of frequencies and amplitudes while acquiring unsteady pressure data would answer these questions and ultimately benefit the prediction of challenging aeroelastic and flow phenomena.

Such a forced oscillation system has been designed, installed, and tested at the Transonic Dynamics Tunnel (TDT) at NASA Langley

Presented as Paper 2002-0171 at the AIAA 40th Aerospace Sciences Meeting and Exhibit, Reno, NV, 14 January 2002; received 4 April 2002; revision received 8 July 2002; accepted for publication 9 July 2002. Copyright © 2002 by the American Institute of Aeronautics and Astronautics, Inc. The U.S. Government has a royalty-free license to exercise all rights under the copyright claimed herein for Governmental purposes. All other rights are reserved by the copyright owner. Copies of this paper may be made for personal or internal use, on condition that the copier pay the $10.00 per-copy fee to the Copyright Clearance Center, Inc., 222 Rosewood Drive, Danvers, MA 01923; include the code 0021-8669/03 $10.00 in correspondence with the CCC.

*Aerospace Engineer, Aeroelasticity Branch, 226 Dodd Boulevard, MS 340; d.j.piatak@larc.nasa.gov. AIAA Member.
†Systems Engineer, Process Systems Branch.

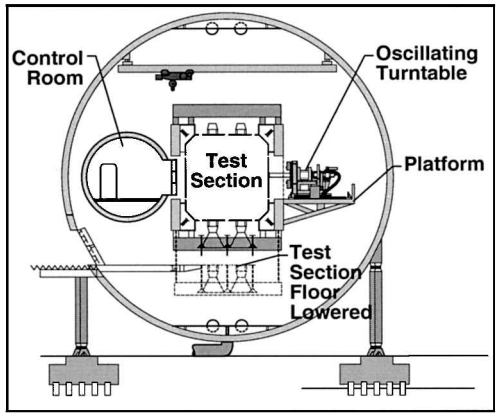

Fig. 1 Cross section of TDT showing test section and location of OTT.

Research Center, Hampton, Virginia, for the purpose of oscillating large, semispan wind-tunnel models in pitch at frequencies up to 40 Hz. The system is known as the Oscillating Turntable (OTT) and can be used to study flow phenomena associated with flutter, LCO, shock dynamics, and nonlinear unsteady aerodynamic effects on a wide variety of aerospace vehicle configurations at transonic speeds. It is anticipated that unsteady pressure measurements resulting from precisely controlled model motions will provide valuable data for computational fluid dynamics (CFD) correlation and aircraft design with respect to unsteady aerodynamic/aeroelastic phenomena.

This paper will discuss the general design and components of the OTT, along with test data from OTT performance testing and from tests of two very different semispan wind-tunnel models. During performance testing, the OTT's hydraulic, electronic, and mechanical systems were evaluated while oscillating an inertia model. The inertia model was designed to simulate the maximum pitch inertia to be oscillated at 40 Hz and 1-deg amplitude. Tests of a small, rectangular, supercritical wing and a large, supersonic transport wing were intended to challenge the OTT over a wide range of operating conditions while acquiring unsteady pressure data. These results will be presented to illustrate OTT performance capabilities, consistency of oscillations, and the usefulness of the OTT as a research tool.

Transonic Dynamics Tunnel Description

The Langley Transonic Dynamics Tunnel (TDT) is a closed-circuit, continuous-flow, variable-pressure, transonic wind tunnel with a 16-ft square test section with cropped corners.[12] The TDT can be operated up to Mach 1.2 at pressures from near vacuum to atmospheric and in either air or heavy gas (R-134a) test mediums. Dynamic pressures up to 550 psf and Reynolds numbers up to 10^6/ft can be achieved in R-134a. Figure 1 is a cross section of the TDT at the test section and shows the relative positions of the plenum, test section, and the location of the OTT. Because of the high-risk nature of dynamic model testing, several features of the TDT have been designed to reduce risk so as to protect the model from destruction and also protect the facility from damage as a result of model debris. These features include a bypass valve system that quickly decreases dynamic pressure and Mach number in the test section to prevent model failure caused by aeroelastic instability, large control room windows for viewing model dynamics, and a tunnel drive fan protection screen designed to prevent model debris from damaging the fan blades.

Oscillating Turntable Description

The OTT is a newly acquired research tool at the TDT that has been designed to oscillate large, semispan models in pitch at high frequencies and transonic conditions. Models can be oscillated sinusoidally at constant or varying frequencies, be subjected to a step input, or undergo user-defined motion. The OTT target oscillatory design points are listed in Table 1, of which design point 1 is the most challenging. Table 2 lists the OTT load limits at the tunnel wall that are large enough to accommodate a wide range of model sizes and test conditions.

Table 1 Performance design points for OTT

Design point	Pitch inertia, lbm-in.^{2}	f, Hz	$\|\alpha\|$, deg
1	65,000	40	1
2	250,000	20	1

Table 2 Maximum steady OTT loads at tunnel wall

Load	Maximum value
Lift	2,400 lbf
Pitching moment	32,000 in.-lbf
Rolling moment	79,000 in.-lbf
Yawing moment	2,700 in.-lbf

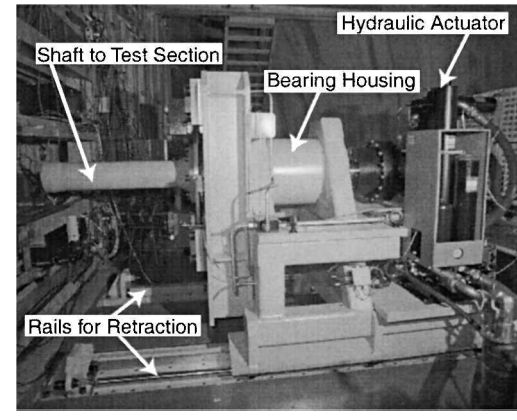

Fig. 2 Side view of OTT.

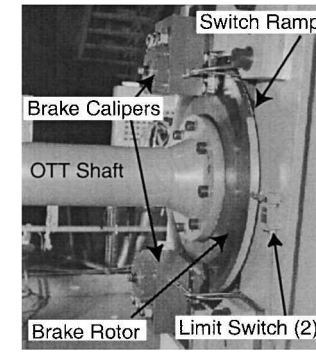

Fig. 3 OTT brake components.

Figure 2 highlights key components of the OTT. The OTT utilizes a powerful rotary hydraulic actuator, rated for 495,000 in.-lbf, and a digital proportional, integral, derivative, feedforward (PIDF) control system to position and oscillate models. Power for the OTT is supplied by a 3000 psi, 150-gpm hydraulic power unit, which is located outside the tunnel pressure shell. Rails allow for precise positioning of the system with respect to the tunnel wall to accommodate a wide range of models and model support systems. Cam wheels and clamps lock the OTT onto its rails once it is in position to prevent the OTT from lifting off the rails during high-power oscillations. For model instrumentation a 2.5-in.-diam hole passes through the center of the entire OTT shaft and actuator to minimize the exposure of this wiring to oscillatory motions.

The OTT also possesses a fast reacting fail-safe braking system to protect a model from excessive aerodynamic forces resulting from uncommanded motion resulting from power or OTT system failures. Figure 3 shows details of the OTT's fail-safe brake system, which include a large-diameter brake rotor, brake calipers, and limit switches that, when tripped, trigger the brake to prevent model overloading or excessive motion. For personnel safety purposes the speed of motion of the OTT is limited to approximately 0.5 deg/s by a flow restriction circuit that is energized while the tunnel door is open.

OTT Shakedown Test Results

The OTT has undergone extensive shakedown tests to determine the performance and reliability of all systems during braking conditions, fault conditions, and a wide range of oscillatory conditions up to frequencies of 41 Hz and oscillation amplitudes up to 10 deg. The inertia model (nonaerodynamic) shown in Fig. 4 possesses a pitch inertia of 65,000 lbm-in.^{2}, which corresponds to design point 1 in Table 1. The inertia model and actuator angular positions were measured using an angular displacement transducer. Also measured was the actuator differential hydraulic pressure, an indication of actuator workload. Table 3 lists the inertial pitching moment for the inertia model and the maximum steady and inertial loads for the two pressure models tested on the OTT.

Using the inertia model just described, performance of the OTT was evaluated through 41-Hz oscillations and is presented in Fig. 5. This figure presents actuator and inertia model oscillatory amplitude and actuator differential hydraulic pressure amplitude ΔP vs frequency for a 1-deg sinusoidal oscillation actuator command. Referring to the actuator and differential pressure amplitude in Fig. 5, the actuator angular amplitude is shown to be nearly 1 deg through 36 Hz, at which frequency the hydraulic system reaches its maximum pressure of 3000 psi. As expected, the actuator cannot maintain the commanded 1-deg-amplitude oscillation beyond 36 Hz. However, beyond 20 Hz the model angular amplitude exceeds the actuator amplitude, ultimately reaching 1.8 deg at 36 Hz. The difference between the model and actuator amplitude is caused by torsional windup of the OTT shaft under high dynamic torque. Therefore, Fig. 5 shows that the OTT oscillatory performance requirement listed in Table 1 for design point 1 is met, albeit, in the presence of shaft windup. This highlights the importance of locating an angular displacement transducer as near to the model as possible to measure its motion accurately.

Table 3 Maximum model aerodynamic and inertial loads about the axis of oscillation

Model	Steady lift force, lbf	Steady pitching moment, in.-lbf	Inertial pitching moment, in.-lbf
Inertia	N/A	N/A	185,452@40 Hz
BSCW	591	1,234	1,377@30 Hz
RSM	2,268	16,965	15,143@10 Hz

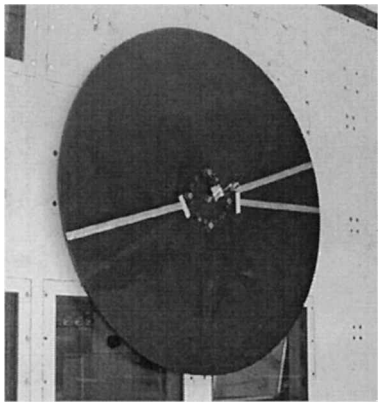

Fig. 4 Inertia model used during OTT shakedown testing.

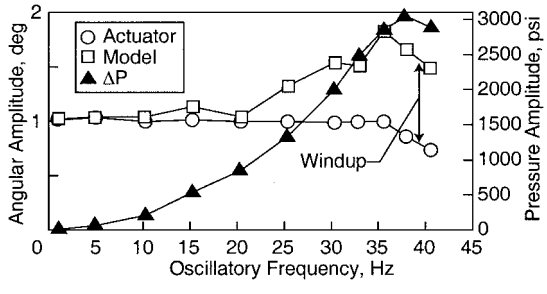

Fig. 5 OTT performance data with inertia model.

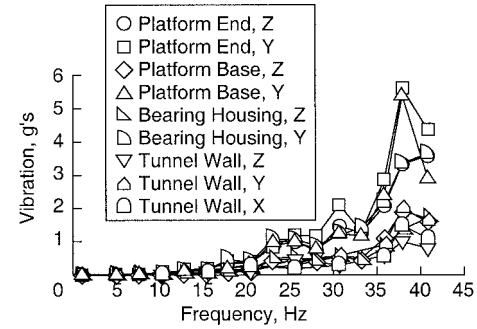

Fig. 6 Platform, OTT, and tunnel wall vibrations during oscillation of inertia model.

Another concern caused by the unique oscillatory capabilities of the OTT is the vibration experienced in the vicinity of the OTT during oscillations. Stress analyses of the platform and test section have identified an 8-g amplitude limit on all platform vibrations for infinite fatigue life. Figure 6 presents vibration amplitude data in g vs OTT oscillatory frequency at various locations in the vertical (Z), lateral (Y), and axial (X) directions with respect to the OTT shaft. Platform vibrations are seen to reach a maximum of 5.5 g at 37 Hz in the lateral direction, and maximum OTT bearing housing vibrations were 3.6 g at 41 Hz in the lateral direction. TDT test section wall vibrations were all below 1.5 g through 41 Hz. As seen in Fig. 6, all vibration levels on the platform were less than the 8-g limit. However, monitoring of platform vibrations is required for OTT oscillatory testing.

OTT Unsteady Pressure Model Test Results

Transonic steady and unsteady pressure measurements have been acquired on two wind-tunnel models at steady angles of attack and during pitch oscillations and step inputs on the OTT in the TDT. Each model was used to address a specific aspect of OTT performance and to acquire a database of unsteady pressures at subsonic and transonic speeds. These tests were designed to quantify OTT performance, reliability, and operational procedures under realistic research conditions and also to demonstrate model instrumentation techniques under the extreme operating conditions of the OTT.

The first model, known as the Benchmark Supercritical Wing (BSCW), is a rectangular semispan wing with a supercritical airfoil and was tested at frequencies up to 30 Hz that challenged the capabilities of the OTT to oscillate a model at high frequencies. Figure 7 shows the BSCW model disassembled and highlights the unsteady pressure measurement locations. Figure 8 shows the BSCW model and splitter plate mounted in the TDT test section. Aerodynamic and inertial loads for this model are listed in Table 3 and are moderate. The second model tested was a large model of a supersonic transport configuration known as the Rigid Semispan Model (RSM), which is shown in Fig. 9. The maximum RSM steady aerodynamic lift listed in Table 3 is near to the lift force limit for the OTT listed in Table 2. The RSM was oscillated at frequencies up to 10 Hz and was intended to test the OTT's ability to oscillate a large model in the presence of large steady aerodynamic loads at moderate frequencies.

Both wind-tunnel models were instrumented with in situ unsteady pressure transducers (±5 psid), which had a quoted repeatability and hysteresis of 0.1%. Prior to testing, all pressure transducers were calibrated at operating temperature in the model using an accurate reference pressure (±0.0025 psi), and before and after each test the calibration of each transducer was verified. Several accelerometers were also mounted within each wing, and an angular displacement transducer (±0.03 deg) was used to measure model position during OTT oscillations.

Unsteady pressure results for both the BSCW and RSM will be presented in plots of mean pressure coefficient $(C_p)_{\text{mean}}$ and real (in-phase) and imaginary (out-of-phase) components of pressure coefficient normalized by oscillation amplitude, $(C_p)_{\text{Re}}$/deg and $(C_p)_{\text{Im}}$/deg, vs nondimensionalized chordwise location x/c. Such data will be presented for various angles of attack $\bar{\alpha}$ and angular

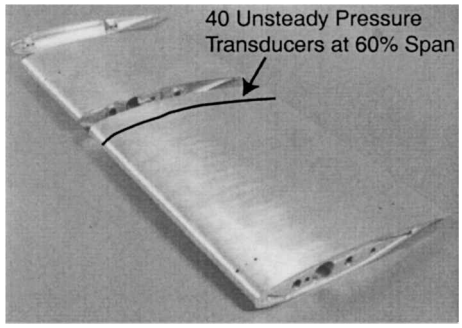

Fig. 7 BSCW model (disassembled) with transducer locations highlighted.

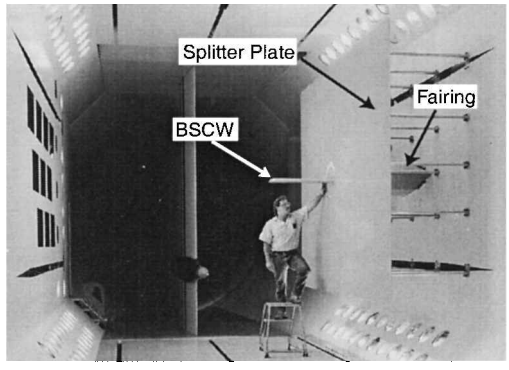

Fig. 8 BSCW model mounted in TDT test section.

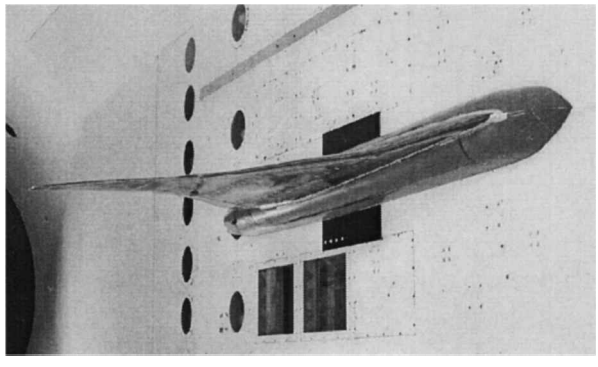

Fig. 9 RSM on the OTT.

amplitudes $|\alpha|$ for oscillatory frequencies f up to 30 Hz. Real and imaginary components of pressure coefficient were obtained from a discrete Fourier transform of pressure coefficient time histories at the oscillatory frequency. Time histories of normalized pressure coefficient at chosen chordwise locations will be presented to illustrate the flow characteristics while the model is undergoing oscillations on the OTT.

BSCW/OTT Test Results

Transonic unsteady pressure measurements have been made on the BSCW while undergoing pitch oscillations at frequencies up to 30 Hz on the OTT. The BSCW has been previously tested at the TDT as part of the Benchmark Models Program.[9,10] The BSCW model has a 32-in. span, 16-in. chord, and a NASA SC(2)-0414 airfoil. The OTT pitch axis was located at $x/c = 0.3$. The spanwise, in-plane, and torsional natural frequencies of the model and support strut were determined to be 24.1, 27.0, and 79.9 Hz, respectively. These natural frequencies dictated decreased oscillation amplitudes at 20 and 30 Hz and the deletion of testing at 25 Hz.

Using 40 in situ transducers, unsteady pressure measurements were made along the chord at the 60% spanwise location at Mach numbers ranging from 0.4 to 0.85 and dynamic pressures of 100, 170, and 200 psf in R-134a heavy gas. Reynolds numbers based on model chord ranged from 2.4 to 6.5×10^6. Boundary-layer transition was fixed at 7.5% chord using a 30 grit strip as it had been in previous tests of this model in heavy gas.[10] Figures 10–15 will present BSCW unsteady pressure results measured during oscillations on the OTT for $f = 1, 5, 10, 15, 20$, and 30 Hz, for $|\alpha| = 0.18$ to 1.0 deg and for $\bar{\alpha} = 0$ and 5 deg. These test conditions correspond to reduced frequencies k ranging from 0.011 to 0.579 for the BSCW. To illustrate the progression of varying degrees of flow nonlinearity, results will be presented at Mach numbers of 0.5, 0.7, and 0.85

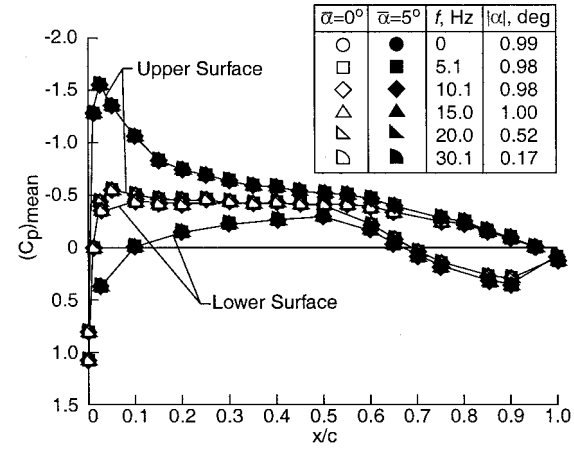

Fig. 10 BSCW mean pressure coefficients for $\alpha = 0$ and 5 deg at $M = 0.5$, $Q = 100$ psf, and $Re = 3.73 \times 10^6$.

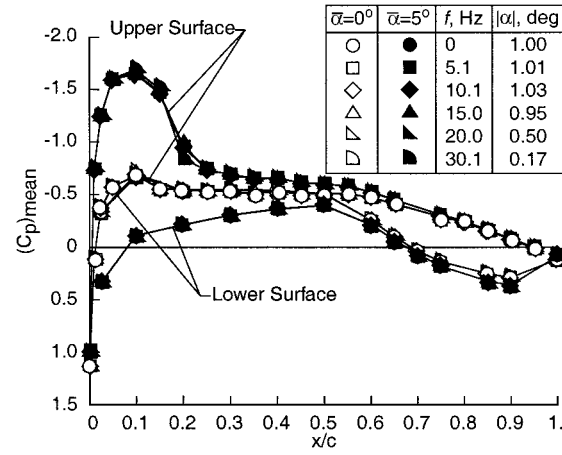

Fig. 11 BSCW mean pressure coefficients for $\alpha = 0$ and 5 deg at $M = 0.7$, $Q = 170$ psf, and $Re = 4.53 \times 10^6$.

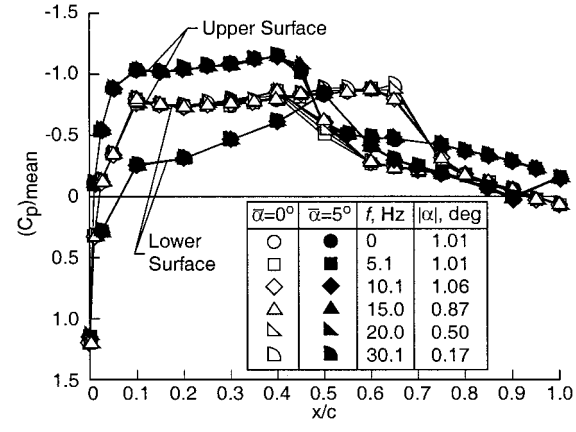

Fig. 12 BSCW mean pressure coefficients for $\alpha = 0$ and 5 deg at $M = 0.85$, $Q = 200$ psf, and $Re = 4.49 \times 10^6$.

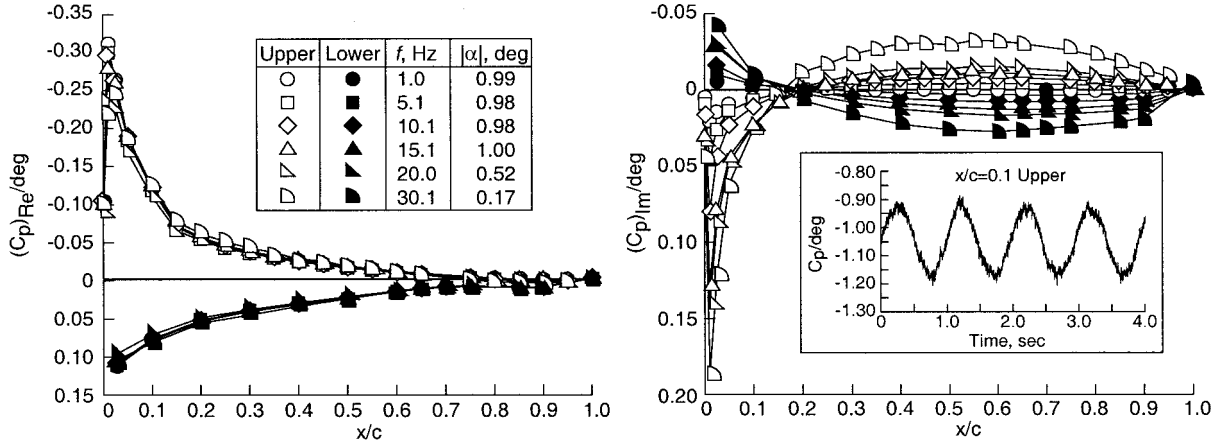

Fig. 13 BSCW real and imaginary pressure coefficients at $\bar{\alpha} = 5$ deg for $M = 0.5$, $Q = 100$ psf, and $Re = 3.73 \times 10^6$.

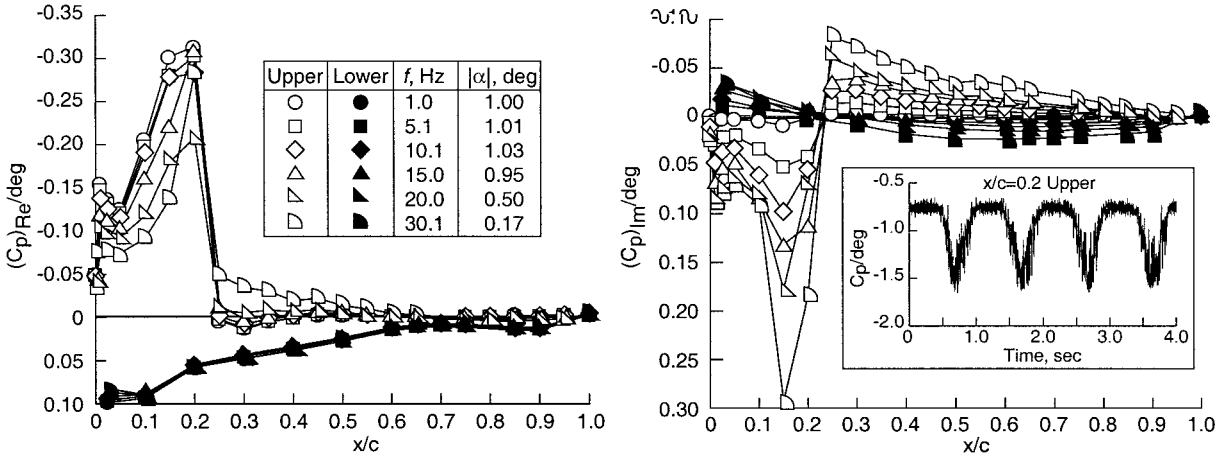

Fig. 14 BSCW real and imaginary pressure coefficients at $\bar{\alpha} = 5$ deg for $M = 0.7$, $Q = 170$ psf, and $Re = 4.53 \times 10^6$.

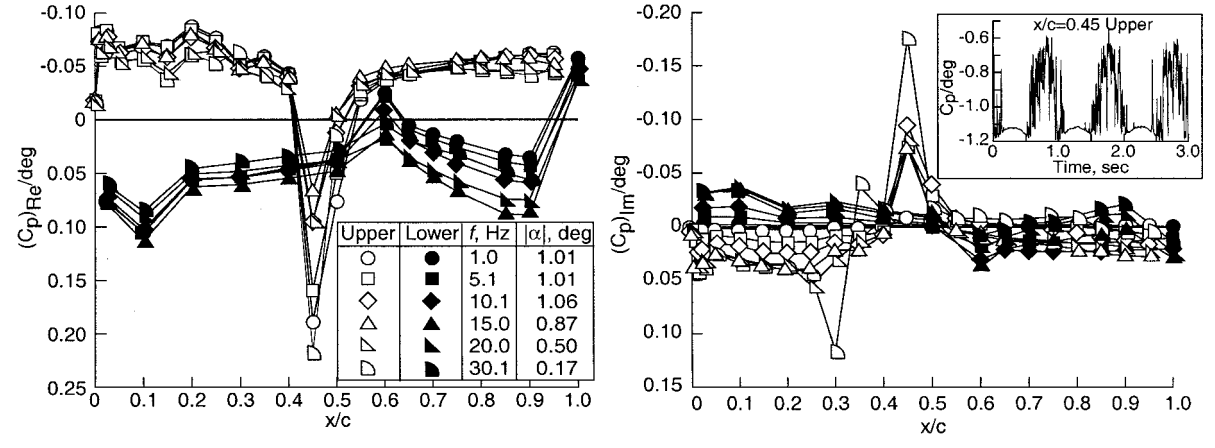

Fig. 15 BSCW real and imaginary pressure coefficients at $\bar{\alpha} = 5$ deg for $M = 0.85$, $Q = 200$ psf, and $Re = 4.49 \times 10^6$.

representing subsonic, moderately transonic, and highly transonic flow. The results are intended to highlight the capabilities of the OTT for the measurement of unsteady pressure data at high frequencies up to transonic conditions.

To illustrate the consistency of OTT oscillations about a mean angle of attack over a large range of test conditions, plots of mean pressure coefficient are presented in Figs. 10–12. These figures illustrate the $(C_p)_{\text{mean}}$ distributions measured during oscillations at frequencies of 0, 5, 10, 15, 20, and 30 Hz at $\bar{\alpha} = 0$ and 5 deg. Figure 10 presents mean pressure coefficient data for test section conditions of $M = 0.5$, $Q = 100$ psf, and $Re = 3.73 \times 10^6$. In this figure the $(C_p)_{\text{mean}}$ distributions for the group of oscillation frequencies at each $\bar{\alpha}$ are identical as expected if the mean angle of attack did not drift during oscillations, the oscillations were consistently sinusoidal, and the oscillation amplitude were sufficiently small. These subsonic pressure coefficient distributions are void of separated flow and shocks and are examples of linear flow cases.

For $M = 0.7$, $Q = 170$ psf, and $Re = 4.53 \times 10^6$, Fig. 11 shows that the $(C_p)_{\text{mean}}$ distributions are identical for the group of oscillation frequencies at each mean angle of attack. The $(C_p)_{\text{mean}}$ distribution for $\bar{\alpha} = 5$ deg in Fig. 11 is an example of moderately transonic flow in which some nonlinear effects would be expected to appear.

The flattened upper-surface pressure coefficient distribution and the presence of a weak shock on the upper surface are characteristics of a supercritical airfoil at transonic speeds and are evident

in Fig. 12 for $M = 0.85$, $Q = 200$ psf, and $Re = 4.49 \times 10^6$. Shocks create adverse pressure gradients as shown in this figure, and it is apparent that for $\bar{\alpha} = 5$ deg a highly nonlinear shock/boundary-layer separated flow case exists. At a given mean angle of attack, $(C_p)_{\text{mean}}$ distributions for each frequency of oscillation are identical or nearly identical in Fig. 12 except in the vicinity of shocks, which have a small localized effect on $(C_p)_{\text{mean}}$. These effects can be expected because the flow in this region is highly nonlinear.

For the oscillations of the BSCW model just discussed, the mean model position during oscillations was held to approximately ± 0.03 deg from the steady angle of attack ($f = 0$). Figures 10–12 provide indirect evidence that the OTT maintained the desired mean angle of attack during oscillations because plots of $(C_p)_{\text{mean}}$ are nearly identical for each frequency.

In Fig. 13 real and imaginary components of C_p/deg are presented at $M = 0.5$, $Q = 100$ psf, $Re = 3.73 \times 10^6$, and $\bar{\alpha} = 5$ deg for $f = 1$, 5, 10, 15, 20, and 30 Hz ($k = 0.015$, 0.076, 0.152, 0.228, 0.305, and 0.457). For this subsonic case the real, in-phase, components are nearly identical for each oscillatory frequency except 20 and 30 Hz at which the amplitudes of oscillation were less than at the other frequencies tested. The imaginary, out-of-phase, components of C_p/deg in Fig. 13 increase linearly as the oscillatory frequency is increased. Also shown in this figure is a time history of C_p/deg for the transducer at $x/c = 0.1$ on the upper surface for a oscillatory frequency of 1 Hz. It shows a nearly sinusoidal response, as expected, at subsonic conditions.

Figure 14 presents unsteady results at $M = 0.7$, $Q = 170$ psf, and $Re = 4.53 \times 10^6$ at $\bar{\alpha} = 5$ deg. Reduced frequencies are 0.011, 0.054, 0.109, 0.163, 0.218, and 0.326, respectively. At this moderately transonic condition a shock is forming at approximately the 15% chord as suggested by the adverse pressure gradient in Fig. 11 for $\bar{\alpha} = 5$ deg. For each oscillatory frequency the real components on the lower surface and the aft upper surface of the airfoil are nearly identical, but on the forward 50% of the upper surface the real components do not align as a result of the presence of the shock. As oscillatory frequency is increased, the imaginary (out-of-phase) components are shown to increase fairly linearly over most of the upper and lower surface of the airfoil. Figure 14 also presents a time history of C_p/deg to illustrate the discontinuity and nonlinearity of the pressure measured at $x/c = 0.2$, where a weak shock is moving across this transducer during oscillations.

Figure 15 shows oscillatory components of C_p/deg at $M = 0.8$, $Q = 200$ psf, and $Re = 4.49 \times 10^6$ for $\bar{\alpha} = 5$ deg, and the highly nonlinear aspects of the flow suggested in Fig. 12 are apparent. Reduced frequencies are 0.009, 0.045, 0.090, 0.135, 0.180, and 0.270, respectively. In Fig. 15 the transonic effects on the flowfield of the BSCW wing are revealed by the peak in $(C_p)_{\text{Re}}$/deg at $x/c = 0.45$ on the upper surface of the wing where a shock has formed and downstream of which the boundary layer separates. This shock is crossing the upper surface transducer at $x/c = 0.45$ as shown in the time history of C_p/deg shown in Fig. 15, which highlights the nonlinear flow characteristics. Such nonlinear shock dynamics are typical in LCOs and flutter at transonic conditions and represent a challenge to unsteady CFD codes. This figure and Figs. 10–14 illustrate the usefulness of the OTT at measuring complex unsteady aerodynamic phenomena on a conventional lifting wing from linear, subsonic flow to highly nonlinear, transonic flow.

RSM/OTT Test Results

The RSM model is a semispan supersonic transport model that has a cranked, delta-wing planform and a 4.86-ft semispan, 11.08-ft root chord, and 7.17-ft mean aerodynamic chord. Tests of the RSM on the OTT were intended to demonstrate OTT capabilities while oscillating a large model at transonic conditions at high angles of attack, which produces large steady and unsteady loads. The maximum steady loads for the RSM, listed in Table 3, are quite large compared to BSCW steady loads. The RSM model was oscillated at frequencies of 1, 2, 5, 8, and 10 Hz at Mach numbers of 0.5–1.05 in an R-134a test medium. Mean angles of attack ranged from -5 to 15 deg and oscillatory amplitudes $|\alpha|$ from 0.2 to 2 deg. Two hundred in situ unsteady pressure measurements at four spanwise

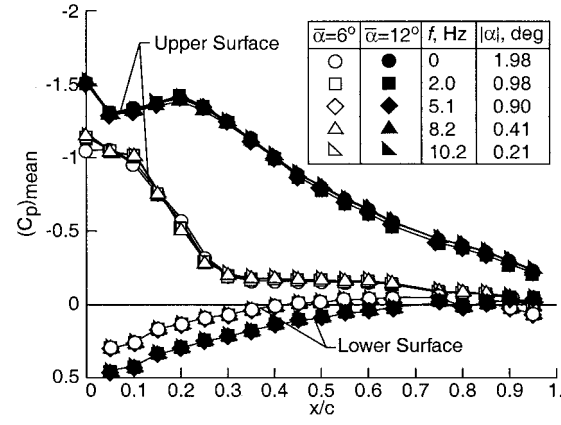

Fig. 16 RSM mean pressure coefficients for $\alpha = 6$ and 12 deg at $M = 0.5$, $Q = 100$ psf, and $Re = 20.5 \times 10^6$.

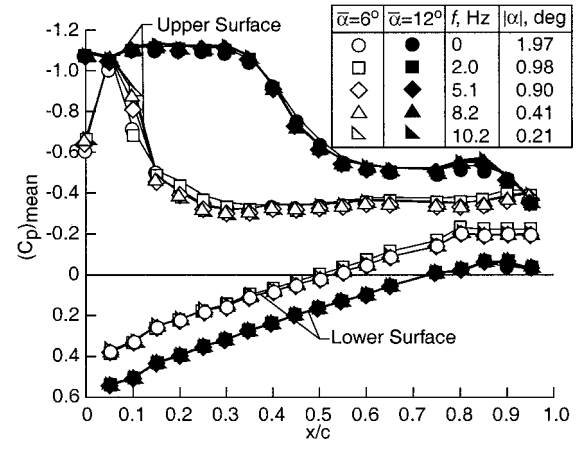

Fig. 17 RSM mean pressure coefficients for $\alpha = 6$ and 12 deg at $M = 1.05$, $Q = 100$ psf, and $Re = 9.8 \times 10^6$.

locations were acquired on the model. Unsteady pressure results for the RSM will be presented for the 60% spanwise location (outboard of the wing crank) for $\bar{\alpha} = 6$ and 12 deg at the following test conditions: $M = 0.5$, $Q = 100$ psf, $Re = 20.5 \times 10^6$ and $M = 1.05$, $Q = 100$ psf, $Re = 9.8 \times 10^6$.

Mean values of the pressure coefficient measured during oscillations of the RSM at $f = 0$, 2, 5, 8, and 10 Hz and at $\bar{\alpha} = 6$ and 12 deg are presented in Figs. 16 and 17 for Mach numbers of 0.5 and 1.05, respectively. The pressure coefficient distributions presented in these figures are typical for a supersonic cranked delta-wing configuration, in which lift is generated to a large extent by vortices created at the wing leading edge. For $M = 0.5$ the mean pressure coefficient distributions at $\bar{\alpha} = 6$ and at 12 deg in Fig. 16 are nearly identical for each oscillation frequency. At the highly loaded conditions of Fig. 17 (Table 3), $(C_p)_{\text{mean}}$ distributions on the upper and lower surface at $\bar{\alpha} = 6$ and at 12 deg are nearly identical for each oscillation frequency. However, some amplitude and/or frequency effects arise in Fig. 17 for $\bar{\alpha} = 6$ deg on the upper surface possibly as a result of the highly vortical flow present.

For the test conditions presented in Figs. 16 and 17, the mean value of model position during oscillations did not vary more than ± 0.03 deg from the steady angle of attack ($f = 0$). These figures provide indirect evidence that the OTT maintained mean angle of attack during oscillations of the RSM under high steady loads because plots of $(C_p)_{\text{mean}}$ are nearly identical for each frequency.

$(C_p)_{\text{Re}}$/deg and $(C_p)_{\text{Im}}$/deg distributions measured on the RSM are shown in Figs. 18 and 19 at the same flow conditions as the preceding figures for $f = 1$, 2, 5, 8, and 10 Hz. The corresponding reduced frequencies at $M = 0.5$ are $k = 0.083$, 0.166, 0.414, 0.662, and 0.828, and for $M = 1.05$ they are $k = 0.038$, 0.077, 0.192, 0.307, and 0.384, respectively. These results are presented to illustrate the

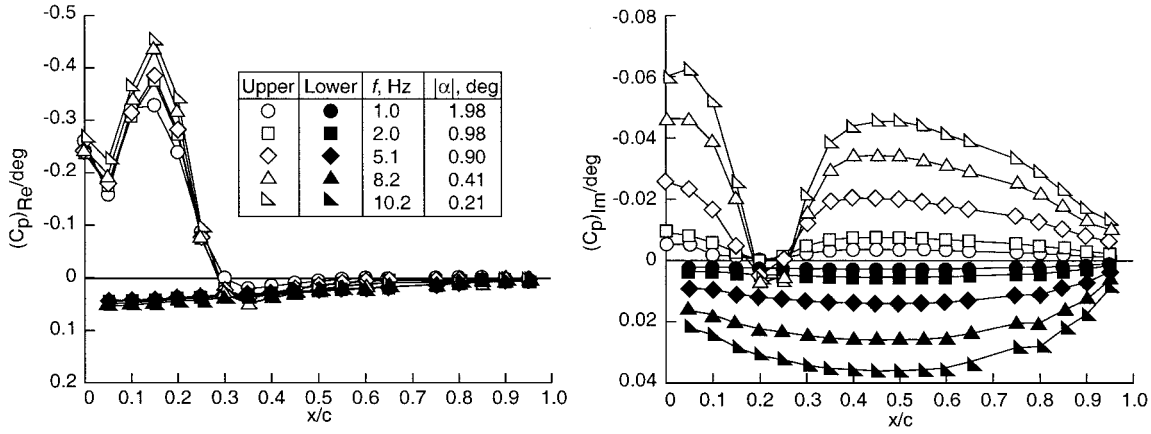

Fig. 18 RSM real and imaginary pressure coefficients at $\bar{\alpha} = 6$ deg for $M = 0.5$, $Q = 100$ psf, and $Re = 20.5 \times 10^6$.

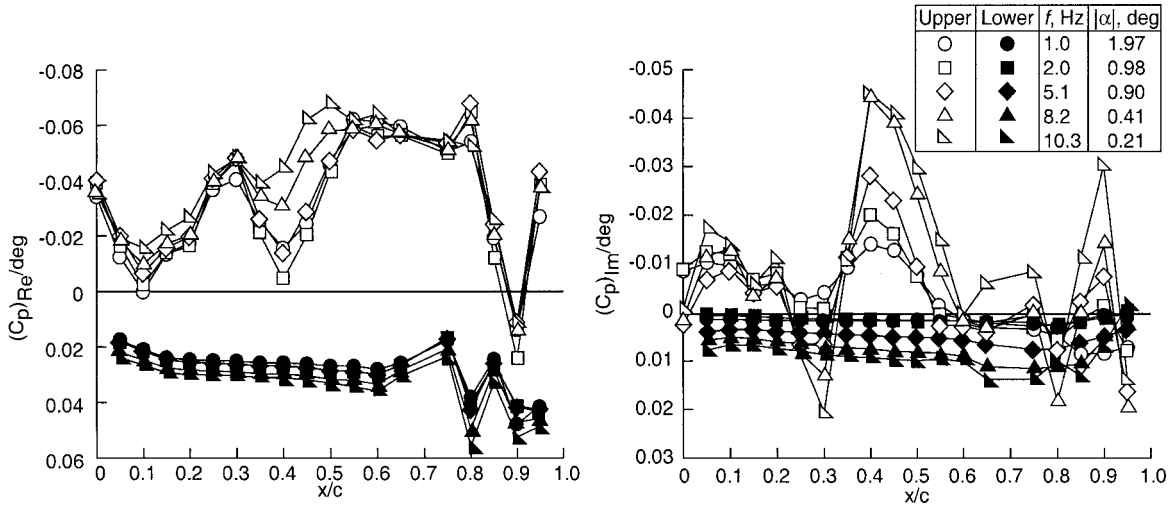

Fig. 19 RSM real and imaginary pressure coefficients at $\bar{\alpha} = 12$ deg for $M = 1.05$, $Q = 100$ psf, and $Re = 9.8 \times 10^6$.

OTT's ability to acquire unsteady data on a large model at moderate and high steady load conditions. The real components of C_p/deg shown in Fig. 18 at $M = 0.5$ and $\bar{\alpha} = 6$ deg are nearly identical on the entire lower surface and the upper surface aft of $x/c = 0.45$. Frequency effects appear to arise on the forward upper surface where $(C_p)_{\mathrm{Re}}$/deg varies with oscillation frequency and the peak in $(C_p)_{\mathrm{Re}}$/deg at $x/c = 0.15$ suggests vortical flow near this location. The imaginary components of C_p/deg are found to vary quite linearly as oscillatory frequency increases, except on the upper surface in the vicinity of $x/c = 0.2$. Also, the upper surface imaginary components exhibit a pronounced decrease in magnitude in the vicinity of the presumed vortex.

Figure 19 shows $(C_p)_{\mathrm{Re}}$/deg and $(C_p)_{\mathrm{Im}}$/deg distributions measured on the RSM at $M = 1.05$ and $\bar{\alpha} = 12$ deg. At this Mach number the real and imaginary components are an order of magnitude smaller for each oscillation frequency as compared to values in Fig. 18 at $M = 0.5$, demonstrating that wing pressures on the RSM at supersonic conditions are less sensitive to model oscillations than at subsonic conditions. Lower surface real components in Fig. 19 follow the same trend for each frequency. Imaginary components appear somewhat linear with respect to oscillation frequency on the lower surface, but not to the same extent on the upper surface. Because a splitter plate was not utilized for the RSM tests, boundary-layer separation effects at this high-angle-of-attack ($\bar{\alpha} = 12$ deg) condition can account for some of the frequency and amplitude effects seen in Fig. 19.

An unforeseen interaction between RSM model dynamics and OTT dynamics was encountered at some tunnel conditions at high angles of attack. In particular, for RSM oscillations at 10 Hz the model's first wing bending mode (22.5 Hz) was visually observed

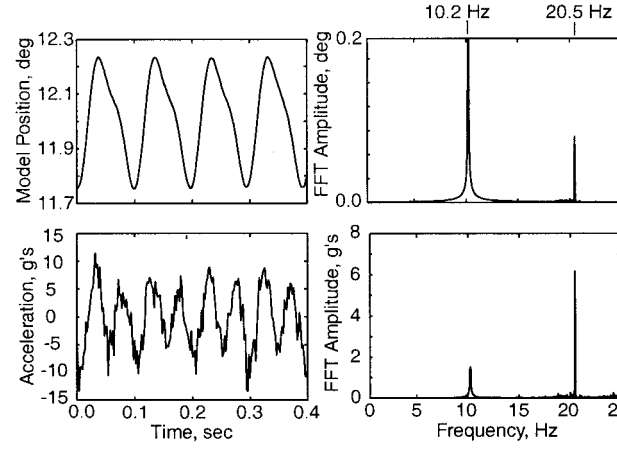

Fig. 20 Time history and FFT of RSM model angular position and wing outboard trailing-edge acceleration at $M = 1.05$, $\bar{\alpha} = 12$ deg, and $f = 10.2$ Hz.

to be excited. This interaction can be seen in Figs. 20 and 21, which present model angular position and wing outboard trailing-edge acceleration time histories and frequency content. For these figures tunnel conditions were $M = 1.05$ and $Q = 100$ psf, and the model was at $\bar{\alpha} = 12$ deg during oscillations at 10.2 and 5.1 Hz, respectively. In Fig. 20 a small "hitch" in the model position time history can be seen, as the model is pitched downward against large steady aerodynamic loads. Because the model angular position time history is not purely sinusoidal, but rather a periodic function that

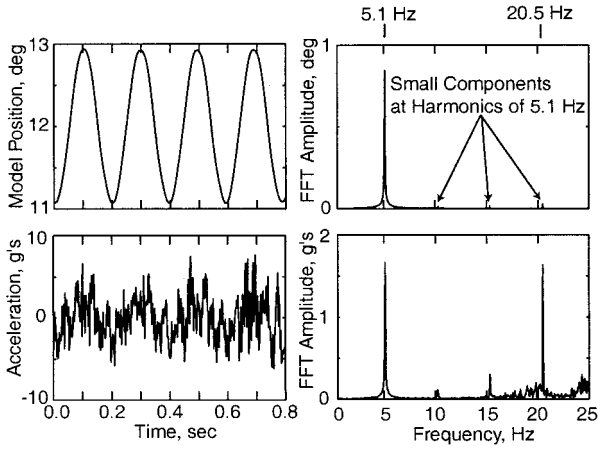

Fig. 21 Time history and FFT of RSM model angular position and wing outboard trailing-edge acceleration at $M = 1.05$, $\bar{\alpha} = 12$ deg, and $f = 5.1$ Hz.

can be represented by a Fourier series, higher harmonics of the oscillation frequency must be present. Referring to the fast Fourier transform (FFT) of model angular position, the 10.2-Hz OTT oscillation frequency is clearly shown in addition to a rather large second harmonic at 20.5 Hz. Additionally, the dominant response of the wing is shown by the outboard trailing-edge accelerometer to be 20.5 Hz as shown in the time history and FFT of Fig. 20. The proximity of the second harmonic at 20.5 Hz to the RSM first bending natural frequency of 22.5 Hz is the cause of this large wing accelerometer response at 20.5 Hz in Fig. 20.

To further illustrate this phenomenon, Fig. 21 presents RSM angular position and outboard trailing accelerometer time histories and FFTs for an oscillation frequency of 5.1 Hz for which several harmonics are present. The model angular position appears to be purely sinusoidal, but small components of higher harmonics of 5.1 Hz arise in the frequency content. As just discussed, these higher harmonics are believed to arise as a result of the high aerodynamic loads present at this condition. In Fig. 21 the fourth harmonic of the 5.1-Hz oscillation frequency is seen to excite a 20.5-Hz response in the outboard trailing-edge accelerometer, again because of its proximity to the 22.5 Hz first wing bending natural frequency. Additional tuning of the OTT closed-loop PIDF control system might alleviate this response. However, this phenomenon indicates that model dynamics must be considered when developing a test program that utilizes the OTT to oscillate a large model that might have a relatively low first natural frequency under high aerodynamic loads.

Conclusions

A new forced oscillation system, known as the Oscillating Turntable (OTT), has been installed and tested at NASA Langley's Transonic Dynamics Tunnel (TDT). The system has been designed to oscillate sidewall-mounted wind-tunnel models instrumented to acquire unsteady pressure and loads data for computational fluid dynamics code validation. Performance testing has shown that the OTT exceeds the original design requirements with respect to oscillatory performance. The hydraulic actuator, hydraulic pump, and digital control system of the OTT have proven reliable during extensive shakedown testing and research model testing. OTT support platform vibrations during high-frequency oscillations of the inertia model were shown to be within its design limits.

Two semispan wind-tunnel tests using the OTT have been conducted that involved the Benchmark Supercritical Wing (BSCW) and the supersonic transport wing known as the Rigid Semispan Model (RSM). These tests were intended to further qualify the OTT as a research tool and to obtain unsteady pressure measurements for the validation of unsteady aerodynamic analyses. A subset of unsteady pressure data from these tests has been presented in this paper to highlight OTT performance and its ability to acquire such data at transonic, high-frequency, and high-load conditions. Conclusions from these tests include the following:

1) The OTT successfully oscillated the BSCW at frequencies up to 30 Hz while holding mean angles of attack.

2) The OTT was proven capable of holding mean angles of attack in the presence of large steady and unsteady aerodynamic loads during oscillations of the RSM at frequencies up to 10 Hz.

3) At transonic conditions for the BSCW, shock dynamics and nonlinear effects that illustrate the usefulness of the OTT at identifying such complex flow phenomena were clearly identified.

4) Instrumentation concepts for OTT testing proved successful during both research tests.

5) Overall performance of the OTT during four weeks of realistic research testing exceeded expectations, and test time was used very efficiently.

6) The potential for interaction between model dynamics and OTT dynamics must be considered.

The BSCW and RSM data acquired on the OTT are available for public dissemination for correlation studies as digitized time histories in a binary file format. Interested parties should contact the author to obtain the subject data.

References

[1]Edwards, J. W., and Malone, J. B., "Current Status of Computational Methods for Transonic Unsteady Aerodynamic and Aeroelastic Applications," AGARD, Paper 1, Oct. 1991.

[2]Bennett, R. M., Dansberry, B. E., Farmer, M. G., Eckstrom, C. V., Seidel, D. A., and Rivera, J. A., "Transonic Shock-Induced Dynamics of a Flexible Wing with a Thick Circular-Arc Airfoil," NASA TM-104088, May 1991.

[3]Nixon, D., *Unsteady Transonic Aerodynamics*, Vol. 120, Progress in Astronautics and Aeronautics, AIAA, Washington, DC, 1989, pp. 2–22, 30–38, and 75–104.

[4]Rainey, A. G., "Measurement of Aerodynamic Forces for Various Mean Angles of Attack on an Airfoil Oscillating in Pitch and on Two Finite-Span Wings Oscillating in Bending with Emphasis on Damping in the Stall," NACA TN 3643, May 1956.

[5]Davis, S. S., and Malcolm, G. N., "Experiments in Unsteady Transonic Flow," AIAA Paper 79-0769, April 1979.

[6]Davis, S. S., and Malcolm, G. N., "Experimental Unsteady Aerodynamics of Conventional and Supercritical Airfoils," NASA TM-81221, Aug. 1980.

[7]Ricketts, R. H., Sandford, M. C., Seidel, D. A., and Watson, J. J., "Transonic Pressure Distributions on a Rectangular Supercritical Wing Oscillating in Pitch," *Journal of Aircraft*, Vol. 21, No. 8, 1984, pp. 576–582.

[8]Cunningham, A. M., Jr., and den Boer, R. D., "Overview of Unsteady Transonic Wind Tunnel Test on a Semispan Straked Delta Wing Oscillating in Pitch," Wright Lab., Flight Dynamics Directorate, WL-TR-94-3017, Wright–Patterson AFB, OH, Aug. 1994.

[9]Bennett, R. M., Eckstrom, C. V., Rivera, J. A., Dansberry, B. E., Farmer, M. G., and Durham, M. H., "The Benchmark Aeroelastic Models Program-Description and Highlights of Initial Results," NASA TM-104180, Dec. 1991.

[10]Dansberry, B. E., Durham, M. H., Bennett, R. M., Rivera, J. A., Silva, W. A., and Wieseman, C. D., "Experimental Unsteady Pressures at Flutter on the Supercritical Wing Benchmark Model," AIAA Paper 93-1592, April 1993.

[11]Rivera, J. A., Dansberry, B. E., Bennett, R. M., Durham, M. H., and Silva, W. A., "NACA0012 Benchmark Model Experimental Flutter Results with Unsteady Pressure Distributions," NASA TM-107581, March 1992.

[12]Cole, S. R., and Garcia, J. L., "Past, Present, and Future Capabilities of the Transonic Dynamics Tunnel from an Aeroelasticity Perspective," AIAA Paper 2000-1767, April 2000.